nature chemical biology

Zebrafish chemical screening reveals an inhibitor of Dusp6 that expands cardiac cell lineages

Gabriela Molina[1,7,8], Andreas Vogt[2,3,8], Ahmet Bakan[4,8], Weixiang Dai[5], Pierre Queiroz de Oliveira[2], Wade Znosko[1], Thomas E Smithgall[1,3], Ivet Bahar[3,4], John S Lazo[2,3], Billy W Day[5,6] & Michael Tsang[1]

The dual-specificity phosphatase 6 (Dusp6) functions as a feedback regulator of fibroblast growth factor (FGF) signaling to limit the activity of extracellular signal–regulated kinases (ERKs) 1 and 2. We have identified a small-molecule inhibitor of Dusp6—(*E*)-2-benzylidene-3-(cyclohexylamino)-2,3-dihydro-1*H*-inden-1-one (BCI)—using a transgenic zebrafish chemical screen. BCI treatment blocked Dusp6 activity and enhanced FGF target gene expression in zebrafish embryos. Docking simulations predicted an allosteric binding site for BCI within the phosphatase domain. *In vitro* studies supported a model in which BCI inhibits Dusp6 catalytic activation by ERK2 substrate binding. We used BCI treatment at varying developmental stages to uncover a temporal role for Dusp6 in restricting cardiac progenitors and controlling heart organ size. This study highlights the power of *in vivo* zebrafish chemical screens to identify new compounds targeting Dusp6, a component of the FGF signaling pathway that has eluded traditional high-throughput *in vitro* screens.

Fibroblast growth factors (FGFs) are members of a large family of secreted glycoproteins that serve important functions in development, proliferation and cellular homeostasis[1]. These ligands bind to single-pass transmembrane proteins of the receptor tyrosine kinase class to activate multiple signaling pathways, including the rat sarcoma homolog (RAS)/mitogen-activated protein kinase (MAPK) cascade[2]. The wide-ranging biological roles of FGFs and the multitude of signaling pathways activated by this family of ligands suggest that FGF signaling must be tightly regulated. Dual-specificity phosphatase 6 (Dusp6; also called MAPK phosphatase 3), Sproutys (Spry1, Spry2, Spry3 and Spry4) and Sef (similar expression to FGFs) proteins function as RAS/MAPK pathway feedback attenuators[1,3]. Through their concerted activities, FGF signaling is adjusted to optimal levels in embryogenesis[1,3]. Sef and Spry proteins suppress RAS/MAPK signaling at multiple points within the pathway, whereas Dusp6 inhibits the pathway only by dephosphorylation of one class of the MAPK family—extracellular signal–regulated kinase (ERK)[1]. Sef, Dusp6 and Sprouty depletion in zebrafish and gene knockout in mice have revealed that the presence of these proteins limits FGF signaling during development and homeostasis[1,4–6]. The identification of small molecules that can reversibly modulate FGF signaling would provide useful tools for dissecting the roles of this pathway in development—a goal that has not been attainable with current genetic methods.

The zebrafish embryo is a vertebrate animal model that is well suited for high-content small-molecule screening[7,8]. Owing to its small size, rapid development and ease of handling, the zebrafish embryo is useful for identifying chemical modulators of signaling pathways *in vivo* and compounds that affect developmental processes[8,9]. Previous zebrafish chemical screens have relied on the observations of phenotypes generated by exposure to small molecules. In one phenotypic screen, dorsomorphin was identified as an inhibitor of bone morphogenetic protein (BMP), as embryos exhibited axial patterning defects upon chemical treatment[10]. Subsequent studies using dorsomorphin in mice have revealed the importance of the BMP pathway in regulating iron metabolism[10]. Another example of the relevance of zebrafish screens is the discovery that prostaglandin E2 is a key regulator of hematopoietic stem cell (HSC) homeostasis[11]. This pathway is conserved in vertebrates, and animal studies have opened the way to using molecules to direct the differentiation of HSCs in order to restore blood deficiencies in humans[11].

The generation of transgenic reporter lines in zebrafish offers alternative *in vivo* tools for chemical screening. Reporters for FGF signaling have been generated and allow for the live visualization of signaling activity during early development[12]. In this study, we performed a chemical screen with an FGF reporter transgenic line and identified a small molecule—(*E*)-2-benzylidene-3-(cyclohexylamino)-2,3-dihydro-1*H*-inden-1-one (BCI, **1**)—that hyperactivates FGF signaling. BCI was first described as a compound that suppresses the transcription factor NF-κB in cell-based luciferase reporter assays[13]. Our analyses revealed that BCI blocks Dusp6 activity in zebrafish embryos and in cultured cells. Molecular modeling predicted an energetically favorable site for BCI binding on the Dusp6 phosphatase domain and suggested a plausible allosteric mechanism of action, which was supported by *in vitro* assays. Using BCI as a chemical probe,

[1]Department of Microbiology and Molecular Genetics, [2]Department of Pharmacology and Chemical Biology, [3]Pittsburgh Molecular Libraries Screening Center, [4]Department of Computational Biology, [5]Department of Pharmaceutical Sciences and [6]Department of Chemistry, University of Pittsburgh, Pittsburgh, Pennsylvania, USA. [7]Present address: SRI International, Center for Advanced Drug Research, Harrisonburg, Virginia, USA. [8]These authors contributed equally to this work. Correspondence should be addressed to M.T. (tsang@pitt.edu).

Received 18 August 2008; accepted 30 April 2009; published online 5 July 2009; doi:10.1038/nchembio.190

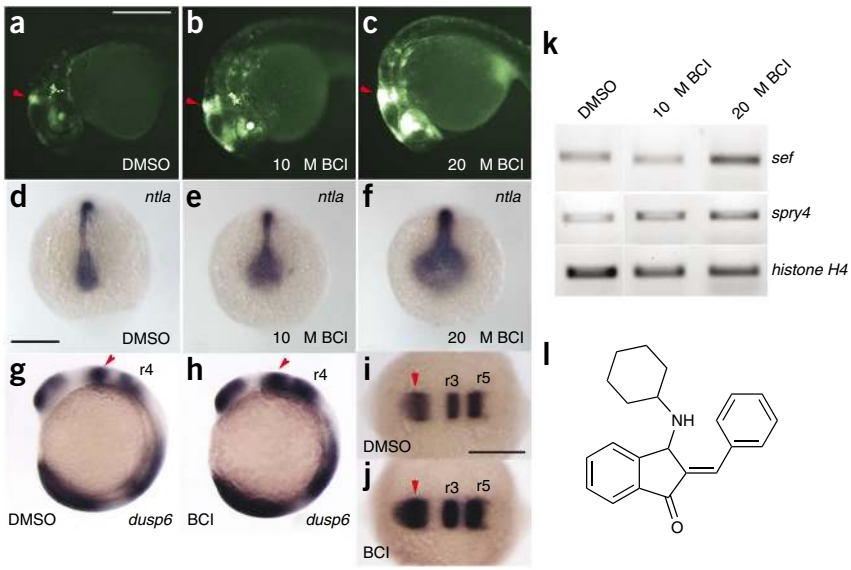

Figure 1 Identification of a small molecule that hyperactivates FGF signaling in zebrafish. (**a**–**c**) *Tg(dusp6:EGFP)*^{pt6} embryos at 30 h.p.f. treated with BCI (**b**,**c**) exhibited increased d2EGFP fluorescence as compared to embryos treated with DMSO (**a**). (**d**–**f**) Embryos treated with BCI during gastrulation had expanded *ntla* expression at the 6-somite stage (**e**,**f**) as compared to DMSO control treatment (**d**). (**g**,**h**) *dusp6* mRNA was increased in BCI-treated embryos. Note that the MHB, r4 and somites showed stronger *dusp6* staining (**h**) than in DMSO-treated embryos (**g**). Red arrowheads demarcate the MHB. (**i**,**j**) BCI treatment during somitogenesis stages expanded the MHB and r3 and r5, as marked by *eng2b* and *egr2b* expression, respectively (**j**) when compared to DMSO treatment (**i**). (**k**) BCI treatment induced expression of the FGF target genes *sef* and *spry4* as measured by RT-PCR. Histone H4 served as RNA loading control. (**l**) The chemical structure of BCI. Scale bars, 250 μm; bar in **d** applies to **d**–**h**.

we found that inhibition of Dusp6 activity during somitogenesis expands cardiac progenitors at the expense of endothelial lineages. These studies suggest that Dusp6 functions as an attenuator of FGF signaling in the cardiac field to regulate heart organ size.

RESULTS

Zebrafish chemical screen identifies an FGF modulator

We previously described the generation of a transgenic zebrafish line, *Tg(dusp6:EGFP)*^{pt6}, that expresses destabilized green fluorescent protein (d2EGFP) under the control of FGF signaling[12]. Using *Tg(dusp6:EGFP)* embryos as a biosensor for FGF signaling, we screened over 5,000 diverse compounds assembled from chemical libraries for small-molecule modulators of this pathway. Five transgenic embryos at 24 h post fertilization (h.p.f.) were arrayed into each well of a 96-well plate containing test compounds at 10 μM. d2EGFP intensity in treated embryos was visually analyzed and compared to vehicle control (0.5% DMSO) after 6–8 h. BCI enhanced d2EGFP fluorescence in a concentration-dependent manner and was detected as early as 2 h post treatment (**Fig. 1a**–**c**). To confirm that BCI hyperactivated FGF signaling, we treated embryos before gastrulation (5 h.p.f.) and analyzed by whole mount *in situ* hybridization the expression of *ntla* (zebrafish *brachyury*), a known FGF target gene[14]. The expression of *ntla* was greatly expanded within the notochord and the tailbud at the 6-somite stage in BCI-treated embryos (**Fig. 1d**–**f**). Similarly, BCI treatment from the 1-somite stage to the 10-somite stage resulted in a marked increase in expression of another FGF target gene, *dusp6*, as shown by the expansion of prospective mid-hindbrain boundary (MHB), rhombomere 4 (r4) and the tailbud (**Fig. 1g**,**h**). The expanded brain structures were confirmed, as BCI increased expression of *engrailed 2b* (*eng2b*), which labels MHB, and *egr2b*, which demarcates r3 and r5 identity, consistent with previous observations from FGF bead implantation studies (**Fig. 1i**,**j**)[15]. To further demonstrate that BCI treatment hyperactivated FGF signaling, we measured an increase in the expression of *il17rd* (also called *sef*) and *spry4* by semiquantitative RT-PCR (**Fig. 1k**; $n = 3$ for each gene)[16–18]. These results confirmed that BCI enhanced FGF signaling in the zebrafish embryo, resulting in the increased transcription of several FGF target genes.

We next determined the BCI structural features required to enhance FGF signaling (**Fig. 1l**). We synthesized two analogs: (*E*)-2-benzylidene-2,3-dihydro-1*H*-inden-1-one (BI, **2**), which lacks the cyclohexylamino group, and 3-(cyclohexylamino)-2,3-dihydro-1*H*-inden-1-one (ICD, **3**), which lacks the benzylidene group (see **Supplementary Methods** for synthesis). The cyclohexylamino and benzylidene substituents were both required in enhancing d2EGFP fluorescence, as analogs lacking either group were inactive (**Fig. 2**).

BCI inhibits Dusp6

To determine the mechanism for BCI's activity and to identify a potential target, we probed where this compound acts within the RAS/MAPK pathway. In BCI-treated transgenic embryos, increased d2EGFP expression was restricted to embryonic regions where FGFs are expressed (**Fig. 1b**,**c**). Furthermore, BCI treatment did not induce d2EGFP expression in the MHB of *Tg(dusp6:EGFP);ace* mutant embryos, which are deficient in Fgf8 signaling (**Fig. 3a**–**d**)[19]. Thus BCI did not enhance FGF signaling in the absence of ligand. We reasoned that BCI could block a feedback attenuator of the FGF pathway, thereby resulting in a net increase in transcription of target genes (**Fig. 3e**). To test this model, we determined whether BCI could rescue

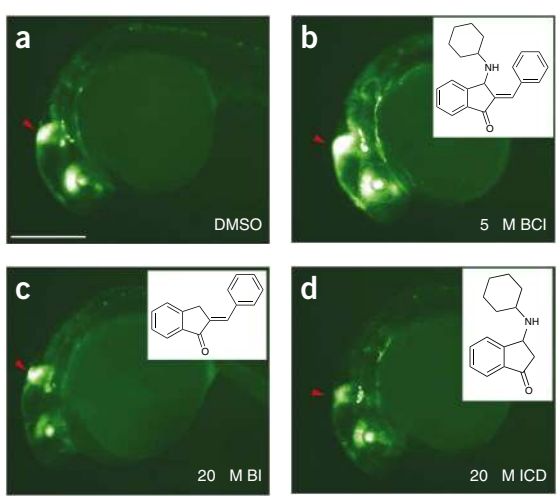

Figure 2 BCI structure-activity relationship studies. (**a**–**d**) Lateral views of 30 h.p.f. *Tg(dusp6:EGFFP)*^{pt6} embryos treated with DMSO (**a**), BCI (**b**), BI (**c**) and ICD (**d**). d2EGFP fluorescence was enhanced in BCI-treated embryos (**b**), whereas related analogs, shown in inner panels, had no effect, even at fourfold higher concentrations (**c**,**d**). Red arrowheads mark MHB. Scale bar, 250 μm.

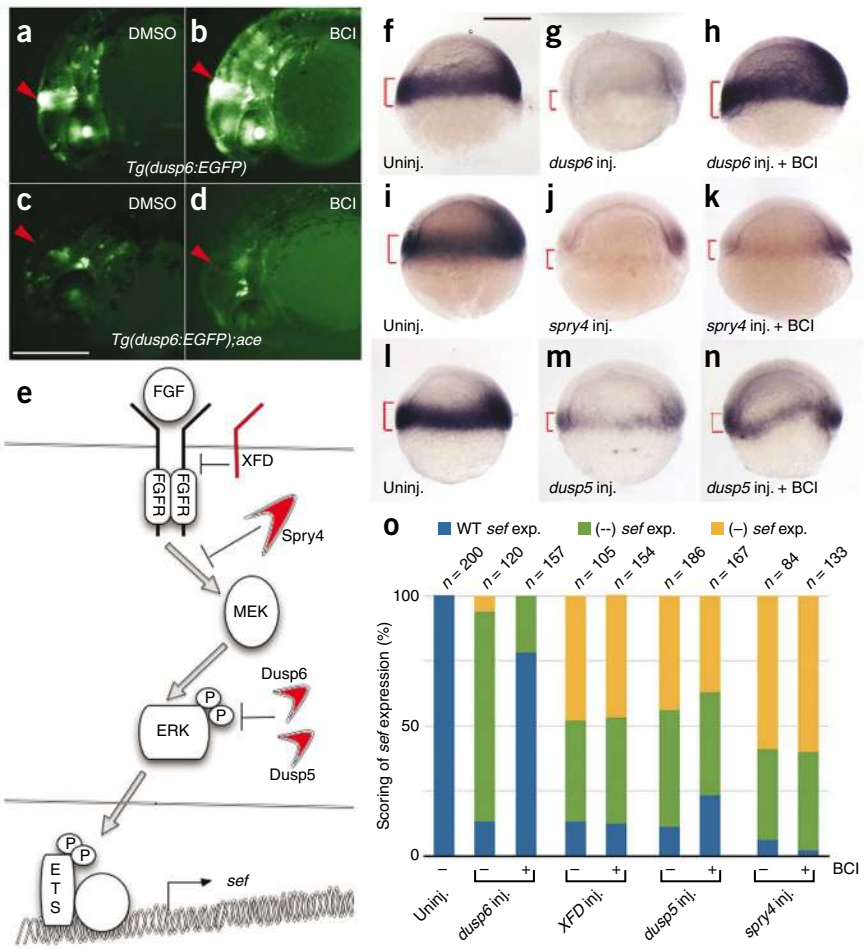

Figure 3 BCI activity require FGF ligand, and BCI inhibits ectopic expression of Dusp6. (**a**–**d**) Lateral views of 30 h.p.f. embryos. *Tg(dusp6:EGFP)*^{pt6} embryos (**a**,**b**) and *Tg(dusp6:EGFP)*^{pt6}*;ace* embryos (**c**,**d**) were treated with BCI (10 μM). The *ace* mutants did not exhibit induction of d2EGFP within the MHB (red arrows), where FGF ligands are not present (**d**). (**e**) Schematic of FGF/RAS/MAPK pathway showing where XFD, Spry4 and Dusp act to block signaling. (**f**–**n**) Lateral views of shield-stage embryos showing *sef* expression by *in situ* hybridization. Red brackets demarcate *sef* expression domain. Injection (inj.) of *dusp6*, *spry4* or *dusp5* reduced *sef* expression (**g**,**j**,**m**), compared to that in uninjected (uninj.) control embryos (**f**,**i**,**l**). BCI treatment restored *sef* expression in *dusp6*-injected embryos (**h**), but not in embryos injected with *spry4* or *dusp5* (**k**,**n**). (**o**) Graph depicting injection and BCI treatment results. *Sef* expression in mRNA-injected embryos is represented by color bars that denote normal (WT) expression in blue, weaker (–) expression in yellow and absent (--) expression in green. Scale bars, 250 μm.

phenotypes generated by ectopic expression of the FGF inhibitors Spry4 and Dusp6 and of the dominant negative receptor XFD in zebrafish (**Supplementary Fig. 1a**)[16,18]. Injection of mRNA encoding *dusp6*, *spry4* or *XFD* into 1-cell-stage zebrafish embryos decreased *sef* expression (**Fig. 3g–o** and **Supplementary Fig. 1c**). The addition of 5 μM BCI to *dusp6*-injected embryos rescued *sef* expression to control levels or higher (**Fig. 3h**,**o**). In contrast, BCI treatment did not reverse the effects of *spry4* or *XFD* mRNA, which suggests that BCI directly inactivated Dusp6 (**Fig. 3k**,**o** and **Supplementary Fig. 1d**). To determine whether BCI could inhibit other Dusps, we first characterized zebrafish *dusp5* and investigated whether it could suppress FGF signaling the same way *dusp6* suppresses FGF signaling[20,21]. Dusp5 has been shown to dephosphorylate activated ERK (pERK), and ectopic expression of zebrafish *dusp5* inhibited *sef* transcription (**Fig. 3m**,**o**)[22]. In contrast to observations with *dusp6* mRNA microinjections, BCI had little or no effect in reversing the phenotype caused by Dusp5 overexpression (**Fig. 3n**,**o**). These observations indicate that BCI is specific for Dusp6. Although both Dusp6 and Dusp5 can dephosphorylate pERK and are highly conserved, their catalytic activities are quite different[22,23]. Dusp6 phosphatase activity is subject to substrate binding and can be catalytically stimulated by ERK interaction[22,23]. This substrate-induced catalytic activity has been described for several members of the Dusp family, including Dusp1 (which is sensitive to BCI, as shown below) and Dusp4 (refs. 23–25). In contrast, Dusp5 is constitutively activated, and substrate binding has little consequence for catalytic rate[22]. Thus the difference we noted in the ability of BCI to rescue Dusp6 but not Dusp5 overexpression *in vivo* suggests that BCI might suppress the activation of Dusp6 associated with substrate binding.

Given that Dusp6 directly dephosphorylates pERK, BCI should restore pERK levels in cells overexpressing Dusp6. We tested this hypothesis in a cell-based chemical complementation assay[26,27] in which HeLa cells were transiently transfected with Myc-tagged human Dusp6 (Dusp6-Myc), stimulated with 12-*O*-tetradecanoylphorbol-13-acetate (TPA, **4**) and immunostained with antibodies to c-Myc (**Fig. 4a**,**b**) and antibodies to pERK (**Fig. 4c**,**d**). Upon TPA treatment, the RAS/MAPK pathway was activated; this led to strong pERK staining in untransfected cells, whereas in cells expressing Dusp6-Myc (**Fig. 4a**), pERK staining was abolished (**Fig. 4c**). BCI treatment of Dusp6-Myc–transfected cells restored pERK levels after TPA addition, which suggests that BCI directly suppresses Dusp6-Myc function (**Fig. 4d**). In this assay, BCI also inhibited human Dusp1, whose catalytic activity, like Dusp6, is induced by substrate binding (**Fig. 4e**)[25]. Half-maximal inhibitory concentration (IC_{50}) values for DUSP6 and DUSP1 inhibition from six independent experiments were 12.3 ± 4.0 μM and 11.5 ± 2.8 μM, respectively, which is consistent with hyperactivation of FGF signaling and d2EGFP expression at these concentrations in the zebrafish embryo (**Fig. 4e**). In contrast, treatment with ICD did not block Dusp6 or Dusp1 activity in the chemical complementation assays (**Fig. 4e**). Taken together, we have shown in biological systems that BCI specifically inhibits Dusp1 and Dusp6, but not Dusp5.

We next investigated whether BCI could directly inhibit Dusp6 activity in an *in vitro* pERK2 dephosphorylation assay. Recombinant Dusp6 completely dephosphorylated pERK2 *in vitro* as determined by immunoblotting with pERK-specific antibodies (**Fig. 4f**, lane 3). Addition of BCI prevented Dusp6-mediated pERK2 dephosphorylation as effectively as the generic tyrosine phosphatase inhibitor sodium orthovanadate (**Fig. 4f**, lane 4 and 6). ICD did not block Dusp6 activity, which supports the conclusion that BCI directly inhibited Dusp6 (**Fig. 4f**, lane 5). Because many known small-molecule phosphatase inhibitors exhibit low selectivity, we determined whether BCI could suppress the phosphatase activity of several related phosphatases.

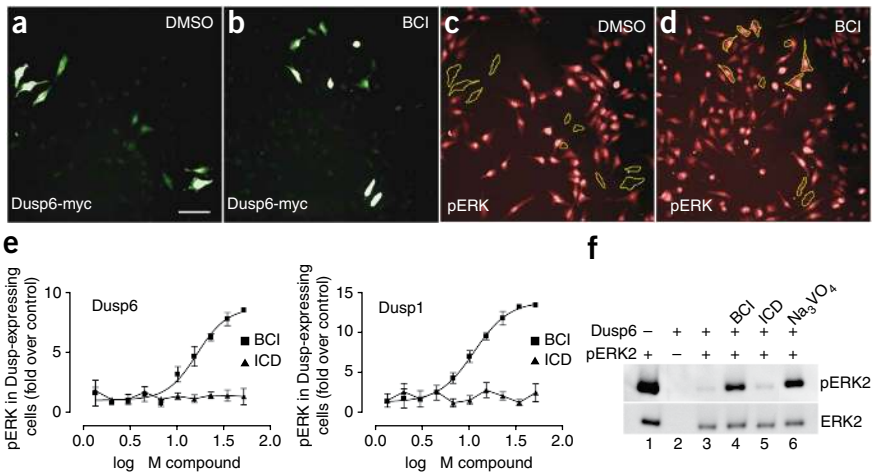

Figure 4 BCI directly inhibits Dusp6 in both chemical complementation and pERK2 dephosphorylation assays. (**a**–**d**) Cell-based chemical complementation assay. HeLa cells transiently transfected with Dusp6-Myc were TPA-stimulated to induced ERK phosphorylation (red cells in **c**,**d**). In cells overexpressing Dusp6-Myc (green cells in **a**), pERK was abolished (**c**; green cells shown in a are shown outlined in yellow). In the presence of BCI, pERK levels remained high (red cells in **d**), even in cells expressing high levels of Dusp6-Myc (**d**; green cells seen in b are outlined in yellow). (**e**) Quantification of pERK levels in Dusp-expressing cells. Cells expressing high levels of Dusp6 (top panel) or Dusp1 (bottom panel) were identified based on c-Myc immunostaining and analyzed for ERK phosphorylation using Kolmogorov-Smirnov statistics as described in the Methods. pERK levels were normalized to Dusp-transfected and vehicle-treated cells. Data are the averages ± s.d. of quadruplicates from a single experiment that was repeated six times with similar results. (**f**) pERK2 *in vitro* dephosphorylation assay shows that BCI (100 μM) specifically suppressed Dusp6 activity (lane 4), whereas a related analog, ICD (100 μM), was inactive (lane 5). Scale bar, 25 μm.

BCI did not block Cdc25B (cell division cycle 25B), PTP1B (protein tyrosine phosphatase 1B) or Dusp3/VHR activity, which indicates that the specificity of BCI is limited to a set of MAPK phosphatases (**Supplementary Fig. 2**).

Computational modeling predicts BCI docking to Dusp6

Crystal structures of several Dusp catalytic domains have been determined[28–31]. In each case, the phosphatase domain encompasses a five- or six-stranded β-sheet surrounded by five α-helices. These structures enabled us to perform unbiased docking simulations[32] to identify potential BCI binding sites (**Supplementary Methods**). BCI was docked onto two different conformations of Dusp6: the low-activity form determined by X-ray crystallography (Protein Data Bank identifier 1MKP)[31] and the high-activity form obtained by homology modeling using ORCHESTRAR (Tripos). From cluster analysis of the resulting BCI-bound conformations, we identified a number of potential binding sites on both the low- and high-activity forms (**Fig. 5a** and **Supplementary Fig. 3**). The most favorable site among them was further assessed by flexible docking[33] using multiple Dusp6 conformations generated by anisotropic network model (ANM) analysis[34] and homology modeling (**Supplementary Methods**). BCI was predicted to preferentially fit within a crevice between the general acid loop and helix α7, rather than interacting directly with the catalytic residues Asp262, Cys293 or Arg299. At this putative binding site, a close interaction of BCI with the backbone of the general acid loop and the side chains of Trp264, Asn335 and Phe336 was predicted (**Fig. 5b**). Further docking simulations using a homology model of Dusp1 showed that BCI-Dusp1 interactions were comparable to those with Dusp6 (**Supplementary Fig. 4a**), thus rationalizing our observed activity data (**Fig. 4e**).

In the zebrafish microinjection assays, BCI inhibited ectopic expression of *dusp6* but not *dusp5*, exhibiting specificity toward certain members of this phosphatase family (**Fig. 3**). We compared the two phosphatase crystal structures to understand how BCI can block Dusp6 but not Dusp5. Structural superposition of Dusp5 and Dusp6 showed that the particular crevice in Dusp6 that accommodates BCI binding is not accessible in Dusp5 (**Fig. 5c**)[22,23,29]. As a result, docking of BCI onto the same region of the Dusp5 phosphatase domain resulted in energetically less favorable interactions (**Supplementary Fig. 4b**). The relative positions of Asp262 and Asp232 in the respective phosphatases Dusp6 and Dusp5 differ by 5 Å after optimal superposition of the two structures, which suggests that their basal activities are determined by the relative location of these catalytic residues (**Fig. 5c**)[29]. It was postulated that substrate binding to Dusp6 induces a conformational shift that reorients Asp262 toward the phosphatase loop, thereby creating a high-activity enzyme[35]. In support of this model, mutation of Asp262 to asparagine did not abolish basal phosphatase activity, but suppressed catalytic activation upon ERK binding[31]. To further understand BCI action on Dusp6 mechanistically, we explored Dusp6 dynamics by particularly focusing on the ANM modes that induce conformational changes at the general acid loop. Our analysis showed that Dusp6 has an intrinsic, structure-induced tendency to suitably reorient its general acid loop to position Asp262 closer to the phosphatase loop (**Supplementary Movies 1** and **2**)[36]. Therefore, we proposed that BCI binding to the accessible crevice in the low-activity form effectively blocks the flexibility of this loop, thereby preventing the interaction of Asp262 with the other catalytic residues. Such constraints on functional motions are likely to inhibit Dusp6 activation induced by ERK binding.

BCI inhibits ERK2-mediated activation of Dusp6

To test these modeling predictions, we measured the dephosphorylation of a small-molecule phosphatase substrate, 3-*O*-methylfluorescein phosphate (OMFP, **5**), by Dusp6 in the presence and absence of ERK2. Docking simulations predicted that BCI and OMFP could simultaneously bind within the phosphatase active site, with OMFP interfacing with the core catalytic residues (**Supplementary Fig. 5a**). This suggests that BCI would not block basal Dusp6 phosphatase activity toward OMFP. Indeed, at a concentration that inhibited ERK dephosphorylation *in vitro* (**Fig. 4f**), BCI did not inhibit basal Dusp6 activity (**Supplementary Fig. 5b**). Addition of ERK2 protein stimulated Dusp6 dephosphorylation of OMFP threefold, and this enhancement was substantially inhibited in the presence of BCI (57% inhibition) (**Fig. 5d**). Increasing the ratio of ERK2 to Dusp6 (10:1) in the activation assay resulted in a sevenfold enhancement that was also suppressed by the addition of BCI (30% inhibition) (**Supplementary Fig. 5c**). These data suggest that BCI is an allosteric inhibitor of Dusp6 that prevents the catalytic stimulation of phosphatase activity induced by substrate binding.

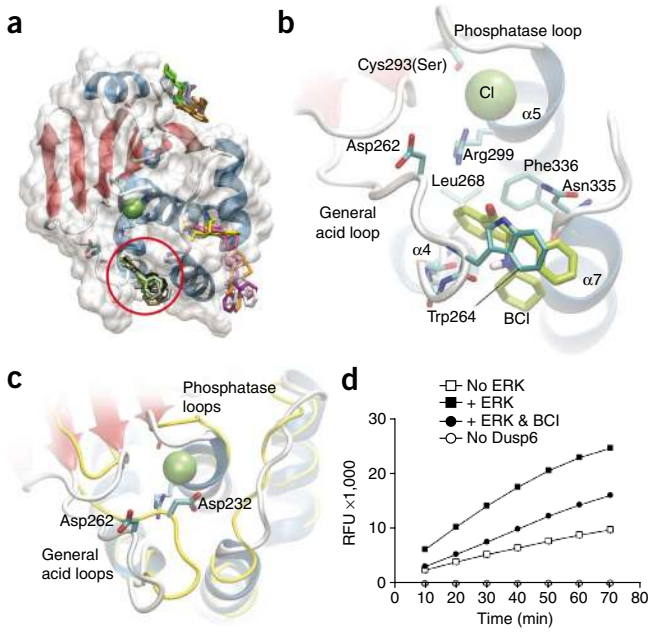

Figure 5 Modeling of BCI-Dusp6 interactions and *in vitro* testing of an allosteric inhibition mechanism. (**a**) Unbiased docking solutions for low-activity conformation of Dusp6 phosphatase domain. Each docking pose corresponding to a cluster of spatially close solutions is colored differently. Clusters in the vicinity of the active site are circled. The catalytic cavity is distinguished by a chloride ion (green). (**b**) Close-up view of BCI (lime green) interactions. In addition to general acid loop backbone, BCI interacts with Trp262, Asn335 and Phe336 side chains. (**c**) Superposition of Dusp5 (yellow) and Dusp6 (white) crystal structures showing that the catalytic acid, Dusp5-Asp232, is positioned approximately 5 Å closer to the catalytic pocket (phosphatase loop) than its Dusp6 counterpart (Dusp6-Asp262). (**d**) ERK2 stimulated Dusp6 dephosphorylation of OMFP, and this induction was blocked by BCI. Relative fluorescence units (RFU) were measured at excitation/emission wavelengths of 485/525 nm.

The role of Dusp6 and FGF in regulating heart size

The identification of a small molecule that blocks the biologically relevant activity of Dusp6 and Dusp1 allowed us to probe the requirement for these enzymes in later developmental processes. Given that BCI could potentially block related members of the Dusp family, we examined the expression of other *dusp* genes in zebrafish. Expression of several *dusp* genes, including *dusp4*, *dusp1*, *dusp7*, *dusp5* and *dusp22a*, has been described in detail (see **Supplementary Methods** and **Supplementary Fig. 6**) (refs. 20,21,37,38; B. Thisse and C. Thisse, direct submission to http://zfin.org/). Of these, only Dusp6 functions as a feedback regulator of FGF/MAPK/ERK signaling and is expressed within the anterior lateral plate mesoderm, thus supporting the idea that this phosphatase has a role in heart development. In early embryogenesis, Dusp6 is an important regulator of FGF signaling; knockdown with antisense morpholino oligonucleotides results in embryo polarity defects, which precludes the study of the role of Dusp6 in later development[18]. In contrast, small molecules permit analysis at later stages of development owing to rapid and transient perturbation of their biological targets.

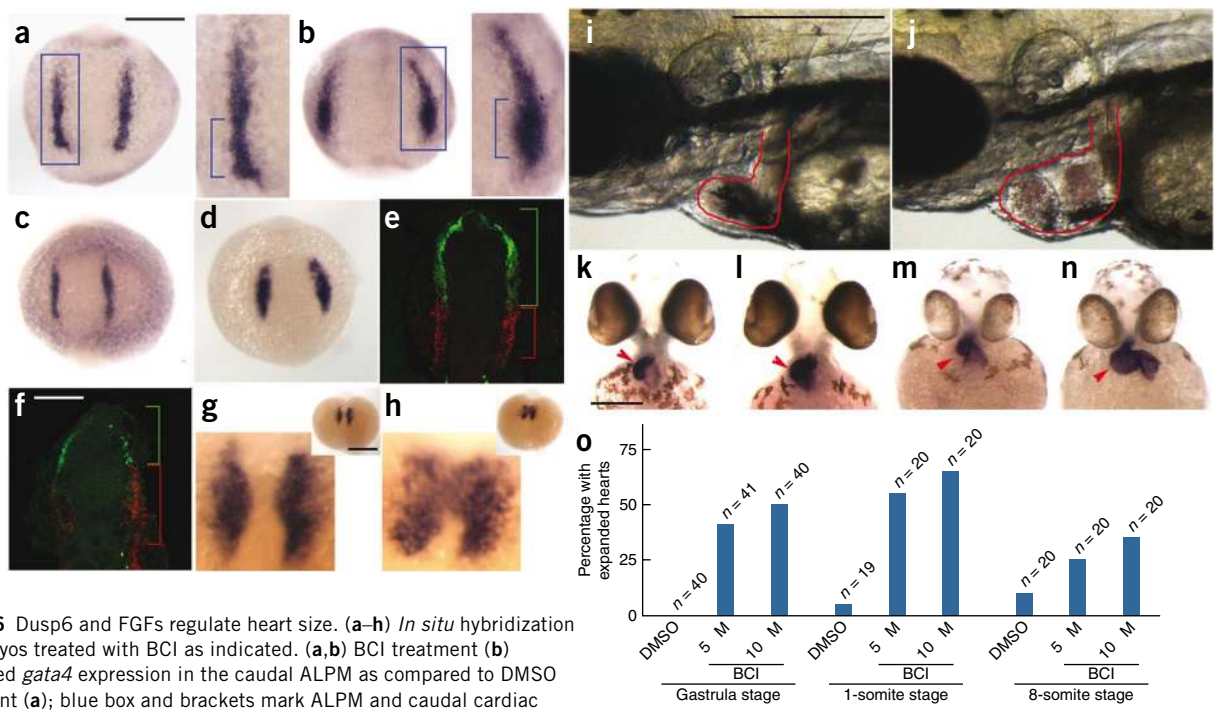

Figure 6 Dusp6 and FGFs regulate heart size. (**a**–**h**) *In situ* hybridization of embryos treated with BCI as indicated. (**a**,**b**) BCI treatment (**b**) expanded *gata4* expression in the caudal ALPM as compared to DMSO treatment (**a**); blue box and brackets mark ALPM and caudal cardiac domain, respectively. (**c**,**d**) BCI increased *nkx2.5* expression and expanded cardiac progenitor populations (**d**) as compared to DMSO control treatment (**c**). (**e**,**f**) Fluorescent double *in situ* hybridization showing *scl* (green) and *hand2* (red) expression in BCI-treated embryos. There is reduction of *scl* expression with a concomitant expansion of *hand2* in BCI-treated embryos (**f**) as compared to control untreated embryos (**e**). Red and green brackets show expression domains. (**g**,**h**) *cmlc2* expression in 18-somite-stage embryos showed an increase in cardiomyocytes in BCI-treated embryos (**h**), as compared to DMSO treated embryos (**g**). (**i**,**j**) Larvae at 56 h.p.f. treated with BCI (from 40% epiboly for 8 h) had enlarged hearts. Red outlines show hearts in embryos treated with control DMSO (**i**) and BCI (**j**). These phenotypes correspond to expansion of *vmhc* (compare **k** to **l**) and *cmlc2* (compare **m** to **n**) staining (red arrowheads). (**o**) Graph showing that temporal inhibition of Dusp6 from the gastrula stage to the somitogenesis stage resulted in cardiac expansion. Scale bars, 250 μm.

Using BCI as a chemical probe, we investigated how inhibiting Dusp6 activity would alter patterning and formation of the heart. The zebrafish heart develops from a small group of cardiac progenitor cells that can be identified by 5 h.p.f. within the mesodermal layer of the blastula-stage embryo[39,40]. During gastrulation, cardiac progenitor cells undergo cellular migration to form two bilateral populations known as the anterior lateral plate mesoderm (ALPM, located just behind the MHB) and begin to express the transcription factors encoded by *nkx2.5* and *gata4* (refs. 40,41). Studies have described a role for Fgf8a in zebrafish heart development. In embryos harboring an *fgf8a* mutation, both atria and ventricular cells are reduced[42,43]. In agreement with the notion that FGF signaling plays a role in stipulating heart size, ectopic expression of a constitutively activated FGF receptor (Fgfr1) during somitogenesis stages expanded cardiac tissue[42]. Therefore, we used BCI to test whether Dusp6 limits FGF signaling and restricts cardiac progenitors and heart organ size. In BCI-treated embryos, a caudal expansion of *gata4* in the ALPM was observed (compare **Fig. 6a** to **Fig. 6b**; 81%, $n = 16$). The *gata4* caudal expansion of the ALPM corresponds to where cardiac progenitors are situated at the 10-somite stage. Examination of *nkx2.5* expression in BCI-treated embryos showed expanded cardiac progenitor pools as compared to DMSO-treated embryos, which confirms a specific effect on heart precursors (compare **Fig. 6c** to **Fig. 6d**; 91%, $n = 11$). Though we noted an expansion of cardiac progenitors, it was not clear if this event was at the expense of other lineages. Recent studies have shown that a repressive interaction occurs between the vascular and hematopoietic precursors on cardiomyocyte progenitors that determines heart organ size[44]. We analyzed expression of *tal1* (also called *scl*), a gene that is expressed in endothelial and blood lineages located within the rostral domain of the ALPM in BCI-treated embryos from the 1-somite stage. Inhibition of Dusp6 resulted in a marked reduction in *scl* expression, which suggests that activation of FGF signaling expanded cardiac tissue at the expense of blood or endothelial progenitors (compare **Fig. 6e** to **Fig. 6f**; 93%, $n = 15$). Likewise, *etv2*, a marker for vascular fate, was also reduced in BCI-treated embryos (data not shown). The loss of endothelial and hematopoietic lineages was coupled with the concomitant expansion of cardiac *hand2* expression at the 10-somite stage (**Fig. 6f**; 32%, $n = 19$). This surplus of cardiac progenitors was also noted at the 18-somite stage by an increase in cells positive for *cardiac myosin light chain 2* (*myl7*, or *cmlc2*), which specifically labels differentiated cardiomyocytes (compare **Fig. 6g** to **Fig. 6h**; 81%, $n = 16$). To test whether the expansion of cardiac progenitors resulted in an increase in heart tissue, we analyzed treated embryos at larval stage. Embryos were treated at 40% epiboly with BCI or DMSO, followed by compound washout the next day. Embryos were then further incubated until they reached 56 h.p.f. In BCI-treated larvae, we noted a marked expansion in cardiac tissue (**Fig. 6i–o**). To define the critical period during which Dusp6 activity limits heart organ size, we treated embryos at the 1- and 8-somite stages. We observed larger hearts at both time points; however, the frequency was reduced in embryos treated at the later stage (**Fig. 6o**). *In situ* analysis with probes for *ventricular myosin heavy chain* (*vmhc*) and *cmlc2* confirmed that treated embryos exhibited enlarged hearts (**Fig. 6l**,**n** and **Supplementary Fig. 7**). Expansion was particularly notable for ventricular tissue, which is known to be sensitive to Fgf8 signaling (**Fig. 6l**)[42,43]. These results indicate that inhibition of Dusp6 by a small-molecule inhibitor can induce an expansion of myocardial progenitors that ultimately increases heart size.

DISCUSSION

The zebrafish embryo offers distinct advantages over traditional *in vitro* and cell-based chemical screens. With the generation of transgenic FGF reporter lines, it is possible to screen for new compounds that modulate this pathway *in vivo*. In addition, live embryo screens allow for the elimination of toxic compounds and molecules that evoke nonspecific effects on embryo differentiation. From a modest screen of approximately 5,000 compounds, we identified BCI, a small molecule that enhances FGF signaling. Subsequent *in vitro* phosphatase assays and docking simulations provided strong evidence that BCI suppresses the ERK-induced activation of Dusp6.

The identification of BCI allowed us to directly probe the role of Dusp6 in heart formation during a critical period when cardiac-specific transcription factors begin to be expressed. The effects of BCI were consistent with studies of global activation of FGF signaling, which resulted in increased cardiac progenitors[42]. Treatment with BCI expanded the cardiac field at the expense of endothelial lineages. The increase in cardiac progenitors resulted in enlarged hearts, which suggests that FGF signaling must be tightly regulated during this period to allow for proper cardiac morphogenesis to occur. The role for Dusp6 in controlling heart organ size is likely conserved with other vertebrates, as disruption of Dusp6 was recently found to cause enlarged hearts in mice[6].

Previous large-scale high-throughput screens for Dusp6 and Dusp1 inhibitors used *in vitro* assays with artificial substrates. Because these assays do not faithfully recapitulate phosphatase activity in a biological context, no specific Dusp6 inhibitors with *in vivo* activity have been identified[45]. The phosphatase catalytic site is highly conserved across all tyrosine phosphatases, and crystal structures have revealed shallow catalytic pockets. These structural features have further hampered the identification of specific small-molecule phosphatase inhibitors[46]. Small molecules targeting Dusp1 identified from *in vitro* screens have exhibited promiscuous activity or have lacked biological activity[47]. However, with the identification of a chemical Dusp inhibitor, it should be possible to rationally design new molecules based on BCI to block substrate-induced Dusp function. This should offer highly specific compounds to probe the role of Dusps in development, and it could potentially provide new agents for treatment of diseases that are dependent on FGF signaling, such as conditions involving wound repair and regeneration[48,49].

METHODS

Zebrafish chemical screens. All procedures involving zebrafish were reviewed and approved by the University of Pittsburgh Institutional Animal Care and Use Committee. *Tg(dusp6:EGFP)*^{pt6} embryos were obtained by natural crossings and incubated at 28.5 °C until they reached 24 h.p.f. Five transgenic embryos were placed into each well of a 96-well plate in 200 µl of E3 (5 mM NaCl, 0.17 mM KCl, 0.33 mM $CaCl_2$, 0.33 mM $MgSO_4$), and a 0.5% (v/v) DMSO solution was added along with compound from each library at 10 µM. The US National Cancer Institute diversity set, a natural products library from MicroSource Discovery Systems and a phosphatase-targeted set from ChemDiv were screened in this study. BCI (also known as NSC150117) was identified as a compound that enhances fluorescence in treated transgenic embryos. Treated embryos were photographed under the same settings for exposure, gain and magnification for each picture using a MZFLIII (Leica) microscope and fluorescent illumination for GFP using endow cube (Chroma). Qimaging software and the Retiga Exi camera (Qimaging) were used to capture the images. Each experiment was repeated three times to show the reproducibility of the assay, and at least four of the five treated embryos exhibited the same phenotype.

Zebrafish mRNA microinjection. *dusp6* and *XFD* mRNA for microinjection studies were generated as previously described[18]. Both Dusp5 and Spry4 open reading frames were amplified by RT-PCR from 24 h.p.f. zebrafish with the following primers: Dusp5 forward, 5′-AACTCGAGGCCATGAAGGTCTCC AGCATAGATTGCCG-3′; Dusp5 reverse, 5′-AATCTAGATTAAGGCAGCGC

AGTTATTGGACTC-3′; Spry4 forward, 5′-ACTCGAGCCATGGAGTCAAGG GTTCCTCACCACATTC-3′; Spry4 reverse, 5′-AATCTAGATCATGAGGCTT GTTTTTCTGGCTGAC-3′.

Amplified PCR products were subcloned into pCS2+ and sequenced verified, and mRNAs were synthesized as described previously. Embryos were injected with 500 pg mRNA at the 1-cell or 2-cell stage, treated with 5 μM BCI at the 1,000-cell stage and fixed at shield stage for *in situ* hybridization.

Chemical complementation assays in HeLa cells. These experiments were carried out essentially as described[27]. HeLa cells were obtained from ATCC and maintained in a humidified atmosphere of 5% CO_2 at 37 °C, DMEM supplemented with 10% (v/v) fetal bovine serum (HyClone), and 1% (v/v) penicillin-streptomycin (Life Technologies, Inc.). Human c-Myc–Dusp6 (pSG5-PYST1) was kindly provided by S. Keyse (Cancer Research UK)[50]. Full-length Dusp1 was subcloned into pcDNA3.1 for ectopic expression in mammalian cells[50]. HeLa cells (2,000) were plated in the wells of a collagen-coated 384-well plate (Falcon Biocoat) in the presence of FuGene 6 (Roche Biosciences) and c-Myc–Dusp6 or c-Myc–Dusp1 as described[27]. After 20 h in culture, cells were treated in quadruplicate wells for 15 min with ten twofold concentration gradients of BCI or ICD and stimulated for 15 min with TPA (500 ng ml^{-1}). Cells were fixed and stained with Hoechst 33342 in 4% (w/v) formaldehyde, permeabilized and immunostained with a mixture of antibodies to pERK (1:200 dilution, Cell Signaling Technology) and antibodies to c-Myc (1:100 dilution, Santa Cruz Biotechnology). Positive pERK and c-Myc–DUSP signals were visualized with secondary antibodies conjugated to AlexaFluor-594 (pERK) and Alexa-488 (c-Myc). Plates were analyzed by three-channel multiparametric analysis for pERK and c-Myc–DUSP intensities in an area defined by nuclear staining using the Compartmental Analysis bioapplication on an ArrayScan II high-content reader (Cellomics). Restoration of ERK phosphorylation by BCI in cells overexpressing Dusp6 was quantified by Kolmogorov-Smirnov statistics as described previously using DUSP-transfected and vehicle-treated control wells[27]. 1,000 individual cells were gated for Dusp–Myc expression based on c-Myc immunostaining and analyzed for ERK phosphorylation. A pERK cumulative distribution function was established for each condition and compared to a reference cumulative distribution function from Dusp-Myc–expressing and vehicle-treated cells. High Kolmogorov-Smirnov values denote large differences in ERK phosphorylation levels compared with vehicle control and indicate suppression of Dusp activity. To quantify restoration of ERK phosphorylation in the Dusp-expressing cells after compound treatment, Kolmogorov-Smirnov values for each condition were normalized to the average Kolmogorov-Smirnov value from four wells transfected with Dusp1 or Dusp6 and treated with vehicle.

Other methods. Detailed materials and methods for *in vitro* phosphatase assays, molecular modeling and chemical synthesis of BCI and related analogs are listed in **Supplementary Methods**.

Accession codes. Protein Data Bank: The low-activity form of Dusp6 was deposited as part of a previous study under accession code 1MKP (ref. 31).

Note: Supplementary information and chemical compound information is available on the Nature Chemical Biology website.

ACKNOWLEDGMENTS

We thank N. Hukriede, M. Rebagliati and I. Dawid for critical reading of the manuscript. We thank M.S. Poslusney for assistance in the syntheses. We thank R. Schultz (Developmental Therapeutics Program, US National Cancer Institute) for providing the National Cancer Institute diversity set and samples of individual compounds. The project described was supported in part by award number R01HL088016 to M.T. from the US National Heart, Lung, and Blood Institute. The content is solely the responsibility of the authors and does not necessarily represent the official views of the National Heart, Lung, and Blood Institute or the National Institutes of Health (NIH). This work was also supported by NIH grants HD053287, CA52995, MH074411 and CA78039, and by the Fiske Drug Discovery Fund.

AUTHOR CONTRIBUTIONS

G.M., A.V., A.B., P.Q.O., W.D., W.Z. and M.T. performed experiments. G.M., A.V., A.B., T.E.S., J.S.L., I.B., B.W.D. and M.T. designed experiments and analyzed data. M.T. wrote the paper with help from A.V., A.B., T.E.S., J.S.L., B.W.D. and I.B.

Published online at http://www.nature.com/naturechemicalbiology/.
Reprints and permissions information is available online at http://npg.nature.com/reprintsandpermissions/.

1. Thisse, B. & Thisse, C. Functions and regulations of fibroblast growth factor signaling during embryonic development. *Dev. Biol.* **287**, 390–402 (2005).
2. Dailey, L., Ambrosetti, D., Mansukhani, A. & Basilico, C. Mechanisms underlying differential responses to FGF signaling. *Cytokine Growth Factor Rev.* **16**, 233–247 (2005).
3. Tsang, M. & Dawid, I.B. Promotion and attenuation of FGF signaling through the Ras-MAPK pathway. *Sci. STKE* **2004**, pe17 (2004).
4. Abraira, V.E. *et al.* Changes in Sef levels influence auditory brainstem development and function. *J. Neurosci.* **27**, 4273–4282 (2007).
5. Li, C., Scott, D.A., Hatch, E., Tian, X. & Mansour, S.L. Dusp6 (Mkp3) is a negative feedback regulator of FGF-stimulated ERK signaling during mouse development. *Development* **134**, 167–176 (2007).
6. Maillet, M. *et al.* DUSP6 (MKP3) null mice show enhanced ERK1/2 phosphorylation at baseline and increased myocyte proliferation in the heart affecting disease susceptibility. *J. Biol. Chem.* **283**, 31246–31255 (2008).
7. Vogt, A. *et al.* Automated image-based phenotypic analysis in zebrafish embryos. *Dev. Dyn.* **238**, 656–663 (2009).
8. Zon, L.I. & Peterson, R.T. *In vivo* drug discovery in the zebrafish. *Nat. Rev. Drug Discov.* **4**, 35–44 (2005).
9. Peterson, R.T., Link, B.A., Dowling, J.E. & Schreiber, S.L. Small molecule developmental screens reveal the logic and timing of vertebrate development. *Proc. Natl. Acad. Sci. USA* **97**, 12965–12969 (2000).
10. Yu, P.B. *et al.* Dorsomorphin inhibits BMP signals required for embryogenesis and iron metabolism. *Nat. Chem. Biol.* **4**, 33–41 (2008).
11. North, T.E. *et al.* Prostaglandin E2 regulates vertebrate haematopoietic stem cell homeostasis. *Nature* **447**, 1007–1011 (2007).
12. Molina, G.A., Watkins, S.C. & Tsang, M. Generation of FGF reporter transgenic zebrafish and their utility in chemical screens. *BMC Dev. Biol.* **7**, 62 (2007).
13. Callahan, J.F. & Chabot-Fletcher, M.C. Inhibitors of transcription factor NF-kB. US patent application WO 99/65495 (1999).
14. Latinkić, B.V. *et al.* The *Xenopus* Brachyury promoter is activated by FGF and low concentrations of activin and suppressed by high concentrations of activin and by paired-type homeodomain proteins. *Genes Dev.* **11**, 3265–3276 (1997).
15. Maves, L., Jackman, W. & Kimmel, C.B. FGF3 and FGF8 mediate a rhombomere 4 signaling activity in the zebrafish hindbrain. *Development* **129**, 3825–3837 (2002).
16. Fürthauer, M., Reifers, F., Brand, M., Thisse, B. & Thisse, C. sprouty4 acts *in vivo* as a feedback-induced antagonist of FGF signaling in zebrafish. *Development* **128**, 2175–2186 (2001).
17. Tsang, M., Friesel, R., Kudoh, T. & Dawid, I.B. Identification of Sef, a novel modulator of FGF signalling. *Nat. Cell Biol.* **4**, 165–169 (2002).
18. Tsang, M. *et al.* A role for MKP3 in axial patterning of the zebrafish embryo. *Development* **131**, 2769–2779 (2004).
19. Reifers, F. *et al.* Fgf8 is mutated in zebrafish acerebellar (ace) mutants and is required for maintenance of midbrain-hindbrain boundary development and somitogenesis. *Development* **125**, 2381–2395 (1998).
20. Qian, F. *et al.* Microarray analysis of zebrafish cloche mutant using amplified cDNA and identification of potential downstream target genes. *Dev. Dyn.* **233**, 1163–1172 (2005).
21. Sumanas, S., Jorniak, T. & Lin, S. Identification of novel vascular endothelial-specific genes by the microarray analysis of the zebrafish cloche mutants. *Blood* **106**, 534–541 (2005).
22. Mandl, M., Slack, D.N. & Keyse, S.M. Specific inactivation and nuclear anchoring of extracellular signal-regulated kinase 2 by the inducible dual-specificity protein phosphatase DUSP5. *Mol. Cell. Biol.* **25**, 1830–1845 (2005).
23. Camps, M. *et al.* Catalytic activation of the phosphatase MKP-3 by ERK2 mitogen-activated protein kinase. *Science* **280**, 1262–1265 (1998).
24. Chen, P. *et al.* Discordance between the binding affinity of mitogen-activated protein kinase subfamily members for MAP kinase phosphatase-2 and their ability to activate the phosphatase catalytically. *J. Biol. Chem.* **276**, 29440–29449 (2001).
25. Slack, D.N., Seternes, O.M., Gabrielsen, M. & Keyse, S.M. Distinct binding determinants for ERK2/p38alpha and JNK map kinases mediate catalytic activation and substrate selectivity of map kinase phosphatase-1. *J. Biol. Chem.* **276**, 16491–16500 (2001).
26. Vogt, A. & Lazo, J.S. Chemical complementation: a definitive phenotypic strategy for identifying small molecule inhibitors of elusive cellular targets. *Pharmacol. Ther.* **107**, 212–221 (2005).
27. Vogt, A. & Lazo, J.S. Implementation of high-content assay for inhibitors of mitogen-activated protein kinase phosphatases. *Methods* **42**, 268–277 (2007).
28. Almo, S.C. *et al.* Structural genomics of protein phosphatases. *J. Struct. Funct. Genomics* **8**, 121–140 (2007).
29. Jeong, D.G. *et al.* Crystal structure of the catalytic domain of human DUSP5, a dual specificity MAP kinase protein phosphatase. *Proteins* **66**, 253–258 (2007).
30. Jeong, D.G. *et al.* Crystal structure of the catalytic domain of human MAP kinase phosphatase 5: structural insight into constitutively active phosphatase. *J. Mol. Biol.* **360**, 946–955 (2006).
31. Stewart, A.E., Dowd, S., Keyse, S.M. & McDonald, N.Q. Crystal structure of the MAPK phosphatase Pyst1 catalytic domain and implications for regulated activation. *Nat. Struct. Biol.* **6**, 174–181 (1999).

32. Morris, G.M. *et al.* Automated docking using a lamarckian genetic algorithm and an empirical binding free energy functions. *J. Comput. Chem.* **19**, 1639–1662 (1998).
33. Jones, G., Willett, P., Glen, R.C., Leach, A.R. & Taylor, R. Development and validation of a genetic algorithm for flexible docking. *J. Mol. Biol.* **267**, 727–748 (1997).
34. Atilgan, A.R. *et al.* Anisotropy of fluctuation dynamics of proteins with an elastic network model. *Biophys. J.* **80**, 505–515 (2001).
35. Owens, D.M. & Keyse, S.M. Differential regulation of MAP kinase signalling by dual-specificity protein phosphatases. *Oncogene* **26**, 3203–3213 (2007).
36. Bahar, I., Chennubhotla, C. & Tobi, D. Intrinsic dynamics of enzymes in the unbound state and relation to allosteric regulation. *Curr. Opin. Struct. Biol.* **17**, 633–640 (2007).
37. Brown, J.L. *et al.* Transcriptional profiling of endogenous germ layer precursor cells identifies dusp4 as an essential gene in zebrafish endoderm specification. *Proc. Natl. Acad. Sci. USA* **105**, 12337–12342 (2008).
38. Kudoh, T. *et al.* A gene expression screen in zebrafish embryogenesis. *Genome Res.* **11**, 1979–1987 (2001).
39. Keegan, B.R., Meyer, D. & Yelon, D. Organization of cardiac chamber progenitors in the zebrafish blastula. *Development* **131**, 3081–3091 (2004).
40. Yelon, D. Cardiac patterning and morphogenesis in zebrafish. *Dev. Dyn.* **222**, 552–563 (2001).
41. Chen, J.N. & Fishman, M.C. Genetics of heart development. *Trends Genet.* **16**, 383–388 (2000).
42. Marques, S.R., Lee, Y., Poss, K.D. & Yelon, D. Reiterative roles for FGF signaling in the establishment of size and proportion of the zebrafish heart. *Dev. Biol.* **321**, 397–406 (2008).
43. Reifers, F., Walsh, E.C., Leger, S., Stainier, D.Y. & Brand, M. Induction and differentiation of the zebrafish heart requires fibroblast growth factor 8 (fgf8/acerebellar). *Development* **127**, 225–235 (2000).
44. Schoenebeck, J.J., Keegan, B.R. & Yelon, D. Vessel and blood specification override cardiac potential in anterior mesoderm. *Dev. Cell* **13**, 254–267 (2007).
45. Ducruet, A.P., Vogt, A., Wipf, P. & Lazo, J.S. Dual specificity protein phosphatases: therapeutic targets for cancer and Alzheimer's disease. *Annu. Rev. Pharmacol. Toxicol.* **45**, 725–750 (2005).
46. Bakan, A., Lazo, J.S., Wipf, P., Brummond, K.M. & Bahar, I. Toward a molecular understanding of the interaction of dual specificity phosphatases with substrates: insights from structure-based modeling and high throughput screening. *Curr. Med. Chem.* **15**, 2536–2544 (2008).
47. Lazo, J.S. *et al.* Novel benzofuran inhibitors of human mitogen-activated protein kinase phosphatase-1. *Bioorg. Med. Chem.* **14**, 5643–5650 (2006).
48. Gurtner, G.C., Werner, S., Barrandon, Y. & Longaker, M.T. Wound repair and regeneration. *Nature* **453**, 314–321 (2008).
49. Lepilina, A. *et al.* A dynamic epicardial injury response supports progenitor cell activity during zebrafish heart regeneration. *Cell* **127**, 607–619 (2006).
50. Dowd, S., Sneddon, A.A. & Keyse, S.M. Isolation of the human genes encoding the Pyst1 and Pyst2 phosphatases: characterisation of Pyst2 as a cytosolic dual-specificity MAP kinase phosphatase and its catalytic activation by both MAP and SAP kinases. *J. Cell Sci.* **111**, 3389–3399 (1998).